Int. J. Electron. Commun. (AEÜ) 175 (2024) 155111

Contents lists available at ScienceDirect

International Journal of Electronics and Communications

journal homepage: www.elsevier.com/locate/aeue

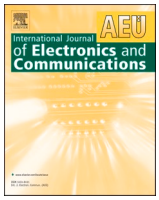

Non-Magnetic Non-reciprocal Bandpass Filter with Quasi-Elliptic Response and Tunable Center Frequency

Girdhari Chaudhary [a], Yongchae Jeong [b,*]

[a] JIANT-IT Human Resource Development Center, Jeonbuk National University, Jeonju-si, Jeollabuk-do 5486, Republic of Korea
[b] Division of Electronic Engineering, Jeonbuk National University, Jeonju-si, Jeollabuk-do 54896, Republic of Korea

ARTICLE INFO

Keywords:
Analytical spectral *S*-parameters
Non-reciprocal bandpass filter (NBPF)
Quasi-elliptic filter response
Time- modulated resonator
Tunable filter

ABSTRACT

This paper presents a detailed analytical numerical design methodology and experimental validation of non-magnetic non-reciprocal bandpass filter (NBPF) that exhibits a highly selective quasi-elliptic response in forward direction of propagation. By modulating resonators with progressive phase shift AC modulation signal, unidirectional RF signal propagation ($|S_{21}| \neq |S_{12}|$) is achieved. Analytical spectral *S*-parameters of the proposed quasi-elliptic NBPF have been derived to gain insight nonreciprocal response. Furthermore, empirical relationships between modulation parameters and filter specifications have also been established through numerical simulations, allowing for simplified design process of the NBPF. By varying the resonant frequency of the resonators, a frequency reconfigurable transfer function can be achieved, providing center frequency tunability of NBPF. For experimental validation purposes, a prototype of microstrip line NBPF is designed and manufactured using three time-modulated resonators, which are implemented using transmission line loaded with varactor diodes. The passband frequency can be continuously tuned by changing DC-bias voltage of varactor diodes. The measurement results revealed that passband center frequency is tuned from 1.65 GHz to 1.95 GHz achieving at tuning ratio of 1.182:1, while maintaining the nonreciprocal behavior with two transmission zeros. For all tuning states, in-band minimum insertion loss in forward direction was measured between 3.20 and 4.8 dB, whereas isolation in reverse direction was measured up to 34.5 dB.

1. Introduction

Non-reciprocal components such as isolators and circulators are crucial components that can protect RF devices from reflected high-power signals or separate transmit and receive channel in in-band full duplex (IBFD) radio [1,2]. However, these nonreciprocal components are typically designed using bulky magnetically-biased ferrite-based resonators [3,4]. Spatio-temporal modulation (STM) is an effective method to achieve nonreciprocity without using bulky magnetically biasing ferrite-based resonators [5]. Recent research efforts are focusing on developing a nonreciprocal bandpass filter (NBPF) that integrates functions of bandpass filter (BPF) and isolator within a single device. STM has proven to be a successful technique for designing NBPF by braking nonreciprocity thorough modulation of resonators with progressive phase shift AC signal. This approach has been demonstrated in both lumped element [6–10] and microstrip-type NBPFs [11–15]. In [16], NBPF was demonstrated using mixed static and time-modulated resonators, however, passband tunability was not achievable in that design. To achieve selective frequency characteristics, NBPFs with a quasi-elliptic transfer function were implemented in subsequent works [17–19].

Despite significant research efforts, none of the works have focused on the analytical *S*-parameter numerical approach solely responsible to insight non-reciprocal scattering parameters. In addition, previously reported NBPFs have primarily relied on parametric studies using harmonic balance (HB) simulations, which can be time-consuming due to convergence requirement of the HB algorithm. In [8], the spectral *S*-parameters of NBPF have been derived, however, these design equations are not applicable for designs that incorporate cross-coupling to achieve quasi-elliptic transfer function.

Aiming to overcome limitations of previously reported NBPFs, this paper presents detailed numerical design approach to design NBPF using time-modulated resonators. To achieve high frequency selective characteristics, quasi-elliptic transfer NBPF is implemented by incorporating cross-coupling between the first resonator and load, which provide low transmission insertion loss and quasi-elliptic filter response with two

* Corresponding author.
E-mail address: ycjeong@jbnu.ac.kr (Y. Jeong).

https://doi.org/10.1016/j.aeue.2023.155111
Received 31 October 2023; Accepted 30 December 2023
Available online 3 January 2024

transmission zeros in forward propagation direction. For the purpose of detailed numerical design, analytical spectral *S*-parameters have been derived. In addition, the proposed design equations allow for insight into the nonreciprocal behavior of the proposed NBPF without use of HB simulations. Furthermore, the proposed numerical design approach can also enable the establishment of empirical relationship between filter specification and modulation parameters, which allow to select optimum modulation parameters. By tuning resonant frequencies of time-modulated resonators, the passband center frequency can be tuned. For proof of concept, microstrip line NBPF with quasi-elliptic response and tunable center frequency is designed, manufactured, and measured. By changing DC-bias voltage of varactor diodes, the passband frequency can be continuously tuned. The proposed NBPF combines functionalities of quasi-elliptic tunable bandpass filter and isolator within single circuit, which can facilitate the development of multi-functional miniaturized RF front end chains for next generation wireless communication systems.

2. Analytical design theory

Fig. 1 depicts coupling diagram and conceptual frequency response of the proposed quasi-elliptic NBPF. RF port 1 is represented by S whereas RF port 2 is denoted by L. RF ports are terminated with normalized impedance of 1 Ω. The proposed NBPF consists of three time-modulated resonators (R_1, R_2, and R_3) where main coupling represented by solid line ($\mathbf{M}_{s1}$, $\mathbf{M}_{12}$, $\mathbf{M}_{23}$ and $\mathbf{M}_{3L}$) and cross-coupling represented by dashed line ($\mathbf{M}_{1L}$). As shown in conceptual transfer function, the proposed filter exhibits two transmission zeros (TZs) in forward direction ($|S_{21}|$) because of cross-coupling between R_1 and output port (L). To achieve a nonreciprocal response, three resonators are modulated with time-varying capacitor of C_i (*t*) as follows [6]:

$$C_i(t) = C_0[1 + m\cos\{\omega_m t + (i-1)\Delta\varphi\}], i = 1, 2, 3 \tag{1}$$

where C_0, $\omega_m = 2\pi f_m$, $\Delta\varphi$, and *m* are nominal capacitance at static state, modulation frequency, progressive phase shift, and the modulation index, respectively.

When RF carrier signal is applied to the time-varying capacitors, a series of intermodulation products are generated. Considering n^{th}-harmonics (i.e., $k_i = \cdots, -2, -1, 0, 1, 2, \cdots$), the spectral admittance matrix (λ_i) of n^{th}-time-modulated resonators is given as (2)

where

$$\Omega_k = \frac{\omega_0}{2\pi \times \Delta}\left(\frac{x_k}{\omega_0} - \frac{\omega_0}{x_k}\right), k = \cdots, -2, -1, 0, 1, 2, \cdots \tag{3a}$$

$$x_k = \omega + k\omega_m, k = \cdots, -2, -1, 0, 1, 2, \cdots \tag{3b}$$

Using coupling diagram shown in Fig. 1(a) and spectral admittance matrix given (2), the spectral *S*-parameters of the proposed quasi-elliptic NBPF are derived as (4). The spectral *S*-parameters shown in (4) can be derived after a series of spectral inverse operations. It should be noted that *S*-parameters shown in (4) no longer possess a single value, instead, each represents a spectral harmonic matrix at each frequency.

$$\mathbf{S}_{11}^{k_1,k_2} = \mathbf{S}_{22}^{k_1,k_2} = U - \frac{2\mathbf{M}_{s1}^2\left(\mathbf{C} + j\mathbf{M}_{3L}^2\lambda_2 - \mathbf{M}_{s1}^2\lambda_3\lambda_2\right)}{\mathbf{A} + j\mathbf{B} - \mathbf{M}_{3L}^2\lambda_1\lambda_2 - \left(\mathbf{M}_{s1}^2 + \mathbf{M}_{1L}^2\right)\lambda_2\lambda_3 - j\lambda_1\lambda_2\lambda_3} \tag{4a}$$

$$\mathbf{S}_{21}^{k_1,k_2} = \frac{2\mathbf{M}_{s1}\left(\mathbf{M}_{12}\mathbf{M}_{23}\mathbf{M}_{3L} - \mathbf{M}_{1L}\mathbf{M}_{23}^2 + \mathbf{M}_{1L}\lambda_2\lambda_3\right)}{\mathbf{A} + j\mathbf{B} - \mathbf{M}_{3L}^2\lambda_1\lambda_2 - \left(\mathbf{M}_{s1}^2 + \mathbf{M}_{1L}^2\right)\lambda_2\lambda_3 - j\lambda_1\lambda_2\lambda_3} \tag{4b}$$

$$\mathbf{S}_{12}^{k_1,k_2} = \frac{2\mathbf{M}_{s1}\left(\mathbf{M}_{12}\mathbf{M}_{23}\mathbf{M}_{3L} - \mathbf{M}_{1L}\mathbf{M}_{23}^2 + \mathbf{M}_{1L}\lambda_3\lambda_2\right)}{\mathbf{A} + j\mathbf{B} - \mathbf{M}_{3L}^2\lambda_2\lambda_1 - \left(\mathbf{M}_{s1}^2 + \mathbf{M}_{1L}^2\right)\lambda_3\lambda_2 - j\lambda_3\lambda_2\lambda_1} \tag{4c}$$

where

$$\mathbf{A} = \mathbf{M}_{s1}^2\mathbf{M}_{23}^2 + \mathbf{M}_{12}^2\mathbf{M}_{3L}^2 + \mathbf{M}_{23}^2\mathbf{M}_{1L}^2 - 2\mathbf{M}_{12}\mathbf{M}_{23}\mathbf{M}_{1L}\mathbf{M}_{3L} \tag{5a}$$

$$\mathbf{B} = \mathbf{M}_{23}^2\lambda_1 + \mathbf{M}_{s1}^2\mathbf{M}_{3L}^2\lambda_2 + \mathbf{M}_{12}^2\lambda_3 \tag{5b}$$

$$\mathbf{C} = \mathbf{M}_{23}^2 - 0.5\mathbf{M}_{12}\mathbf{M}_{23}\mathbf{M}_{3L}\mathbf{M}_{1L} - 4\mathbf{M}_{23}^2\mathbf{M}_{1L}^2 \tag{5c}$$

and *U* is unity matrix. The values of coupling matrix are: $\mathbf{M}_{s1} = M_{s1}U, \mathbf{M}_{12} = M_{12}U, \mathbf{M}_{23} = M_{23}U, \mathbf{M}_{3L} = M_{12}U$, $\mathbf{M}_{1L} = M_{1L}U$. Likewise, ω and ω_0 represents operating angular frequency and center angular frequency, respectively, whereas Δ represents equiripple bandwidth of filter at static state (without modulation). It should be noted that coupling elements ($\mathbf{M}_{s1}$, $\mathbf{M}_{12}$, $\mathbf{M}_{23}$, $\mathbf{M}_3$, $\mathbf{M}_{1L}$) possess the same values at fundamental and harmonic frequencies.

The progressive phase difference ($\Delta\varphi$) plays a crucial role in enabling nonreciprocal response. It is important to note that only central elements in matrices presented in (4) represent the fractional power conversion at

$$\lambda_i = \begin{array}{c} \begin{matrix} k_1 \cdots -2 & & -1 & & 0 & & +1 & & +2 & \cdots \text{ indices} \end{matrix} \\ \begin{bmatrix} \ddots & \vdots & \vdots & \vdots & \vdots & \vdots & \cdots \\ \cdots & \Omega_{-2} & \frac{x_{-2}m}{4\pi\times\Delta}e^{-j(i-1)\Delta\varphi} & 0 & 0 & 0 & \cdots \\ \cdots & \frac{x_{-1}m}{4\pi\times\Delta}e^{j(i-1)\Delta\varphi} & \Omega_{-1} & \frac{x_{-1}m}{4\pi\times\Delta}e^{-j(i-1)\Delta\varphi} & 0 & 0 & \cdots \\ \cdots & 0 & \frac{x_0m}{4\pi\times\Delta}e^{j(i-1)\Delta\varphi} & \Omega_0 & \frac{x_0m}{4\pi\times\Delta}e^{-j(i-1)\Delta\varphi} & 0 & \cdots \\ \cdots & 0 & 0 & \frac{x_{+1}m}{4\pi\times\Delta}e^{j(i-1)\Delta\varphi} & \Omega_{+1} & \frac{x_{+1}m}{4\pi\times\Delta}e^{-j(i-1)\Delta\varphi} & \cdots \\ \cdots & 0 & 0 & 0 & \frac{x_{+2}m}{4\pi\times\Delta}e^{j(i-1)\Delta\varphi} & \Omega_{+2} & \cdots \\ \cdots & \vdots & \vdots & \vdots & \vdots & \vdots & \ddots \end{bmatrix} \begin{matrix} \vdots \\ -2 \\ \\ -1 \\ 0 \\ +1 \\ \\ +2 \\ \vdots \\ k_2 \end{matrix} \end{array} \tag{2}$$

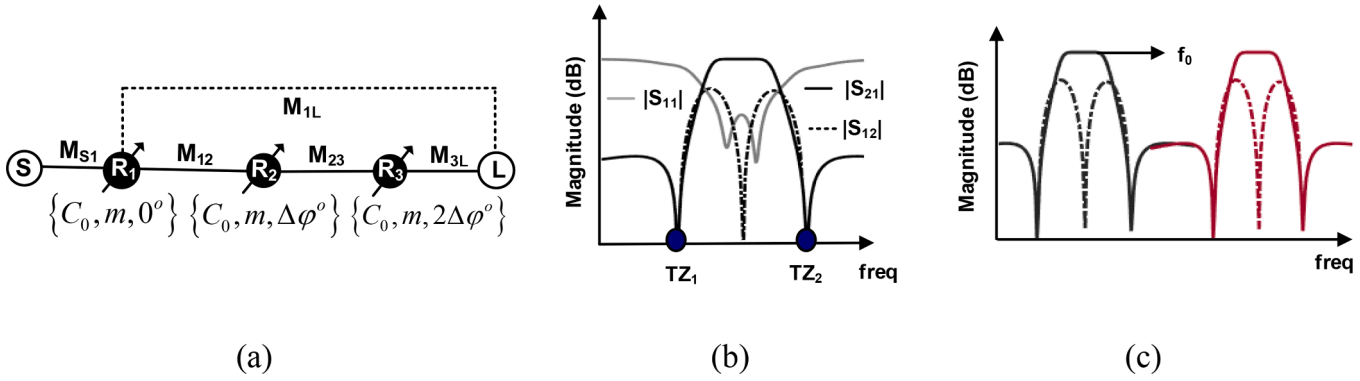

Fig. 1. Proposed quasi-elliptic NBPF: (a) coupling diagram (b) conceptual forward transmission ($|S_{21}|$), reflection ($|S_{11}|$) and reverse isolation ($|S_{12}|$) response of NBPF, and (c) conceptual frequency response of tunable NBPF.

the fundament frequency, while other elements represent the inter-harmonic spectral power conversion. In fact, all elements collectively contribute to achieve nonreciprocal response at the fundamental frequency. When λ_i values of all the resonators are same, the proposed filter provides a reciprocal response resulting in $|S_{21}| = |S_{12}|$.

Fig. 2 shows numerically calculated scattering parameters at fundamental frequency with increasing number of harmonics such as $N_{har} = 5, 7$ (*ie* k_i = -2, -1, 0, +1, +2 and k_i = -3, -2, -1, 0, +1, +2, +3). It can be observed that results are, in general, very stable, showing only small differences as the number of harmonics is increased. Results show that the filter has a flat passband in forward direction with insertion loss (IL) of 0.46 dB and return loss of 16.5 dB. Since the network is lossless, the IL of 0.46 dB in forward direction is due to power that is converted to nonlinear harmonics and is not converted back to the fundamental frequency. As results shown in Fig. 2 also confirm that very strong non-reciprocity in reverse direction is obtained at fundamental frequency. The reverse direction isolation (IX) is higher than 50 dB at center frequency and greater than 7 dB within all frequencies.

Fig. 3(a) shows numerically calculated scattering parameters of the proposed quasi-elliptic NBPF with cross-coupling at fundamental frequency and compared results of NBPF without cross-coupling. The results reveal the generation of two TZs in forward transmission ($|S_{21}|$). These TZs primarily arise from cross-coupling (M_{1L}) between resonator 1 and load. It is noteworthy that when $M_{1L} = 0$, TZs in the forward direction of propagation disappear. Likewise, Fig. 3(b) shows scattering parameters at fundamental frequency when different modulation frequency is selected. Results show that when modulation frequency is selected as $f_m = 1.3\Delta$ where Δ is bandwidth of filter at static state (without modulation), high level of isolation ($|S_{12}|$) with a single null in reverse direction can be achieved. On the other hand, if modulation frequency is selected as $f_m = 1.42\Delta$, reverse isolation with two nulls and slightly wider isolation bandwidth can be obtained, however, magnitude at center frequency is only 20 dB.

2.1. Selection of modulation parameters

To select optimum modulation parameters, the *S*-parameter results are numerically calculated using different modulation parameters (f_m, m and $\Delta\varphi$) and results are shown in Fig. 4. To effectively depict the parameter sweeping results, two data visualization methods, namely line plots, have been used. In these results, colormaps denote the modulation parameters. As observed from these results, the highest reverse isolation (IX = $|S_{12}|$) is achieved when f_m = 130 MHz with acceptable forward insertion loss (IL=$|S_{21}|$). Higher f_m values lead to lower IL, but also lower reverse IX. Regarding modulation index m, higher m leads to higher IX and relatively higher IL. In addition, too large m values provide higher IL and lower IX. When $\Delta\varphi$ is between 65° and 75°, the acceptable lower IL and higher IX is achieved while maintaining the frequency response of NBPF with quasi-elliptic response in forward direction.

Based on these numerical simulation results, an interesting empirical relationship can be established among the modulation parameters (i.e, f_m, m, and $\Delta\varphi$), and filter specifications (i.e, f_0, and Δ = bandwidth of filter when no modulation signal is applied) of the proposed quasi-elliptic NBPF, as given by (6).

$$f_m = 1.30 \times \Delta \tag{6a}$$

$$m = 2.35 \times \Delta / f_0 \tag{6b}$$

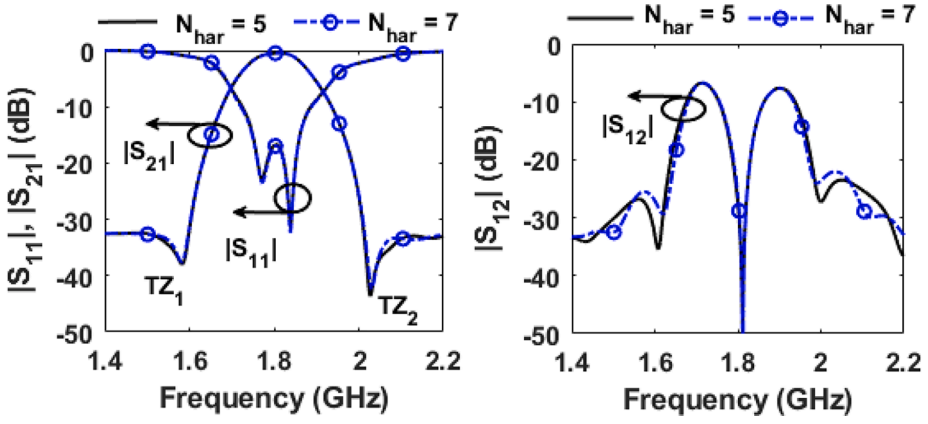

Fig. 2. Numerical simulation results of quasi-elliptic NBPF at f_0 = 1.8 GHz and Δ = 100 MHz with number of harmonics. Coupling matrix values are obtained by optimization and are given as: M_{s1} = 1.3440, M_{12} = 1.3055, M_{23} = 1.4971, M_{3L} = 1.3301, M_{1L} = -0.1120. Progressive phase shift: $\Delta\varphi$ = 75°.

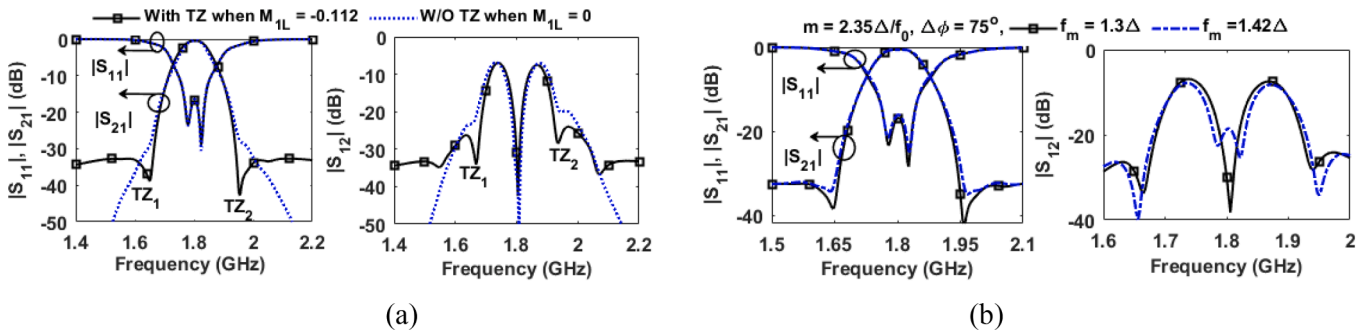

Fig. 3. Numerical simulation results of quasi-elliptic NBPF with $f_0 = 1.8$ GHz and $\Delta = 70$ MHz: (a) with/without TZ, and (b) different modulation frequency (f_m). Coupling matrix values are obtained by optimization and are given as: $M_{s1} = 1.3440$, $M_{12} = 1.3055$, $M_{23} = 1.4971$, $M_{3L} = 1.3301$, $M_{1L} = -0.1120$. Progressive phase shift: $\Delta\varphi = 75^\circ$ and Δ is bandwidth of filter when no modulation is applied.

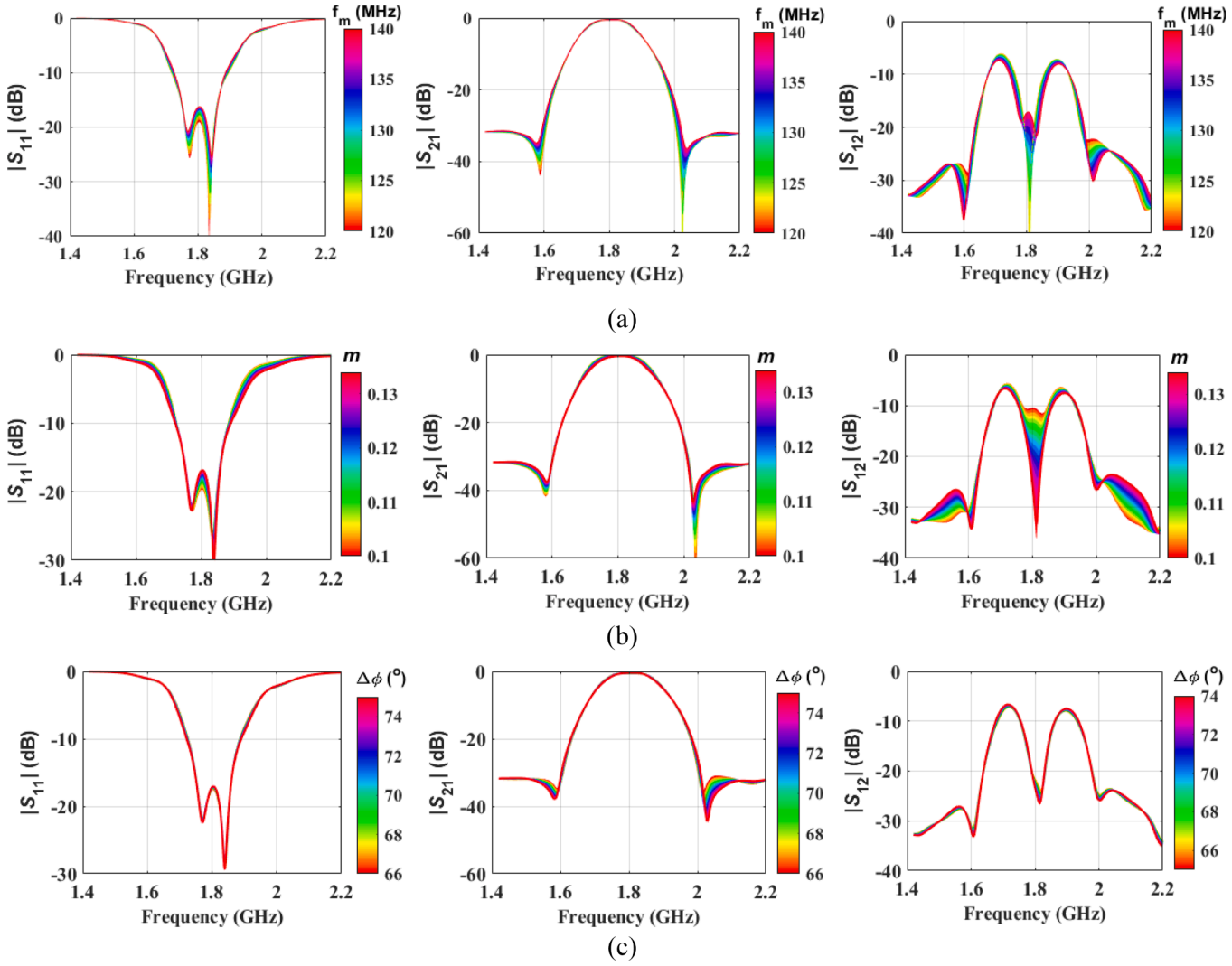

Fig. 4. Numerically calculated frequency response of quasi-elliptic NBPF with modulation parameters (a) different modulation frequency with $m = 0.13$, $\Delta\varphi = 75^\circ$, (b) different modulation index with $f_m = 130$ MHz, $\Delta\varphi = 75^\circ$ and (c) different phase difference with $f_m = 130$ MHz, $m = 0.13$. Coupling matrix values are obtained by optimization and are given as: $M_{s1} = 1.3440$, $M_{12} = 1.3055$, $M_{23} = 1.4971$, $M_{3L} = 1.3301$, $M_{1L} = -0.1120$, $\Delta = 100$ MHz and $f_0 = 1.80$ GHz.

$$65^\circ \leqslant \Delta\varphi \leqslant 75^\circ \tag{6c}$$

It is worth noting that equation (6) provides modulation parameters that enable the design of a quasi-elliptic NBPF with low forward IL and a very high level of reverse isolation. Furthermore, these empirical relations offer a straightforward selection of modulation parameters without need of optimization that can directly be used in experimental verification of fabricated protype of quasi-elliptic NBPF.

Fig. 5 demonstrates the numerically simulated frequency of the proposed quasi-elliptic NBPF for different equiripple bandwidths (Δ) at static state (no modulation). The results reveal that the forward transmission insertion loss (IL= $|S_{21}|$) is $<$ 0.5 dB, reverse isolation (IX = |

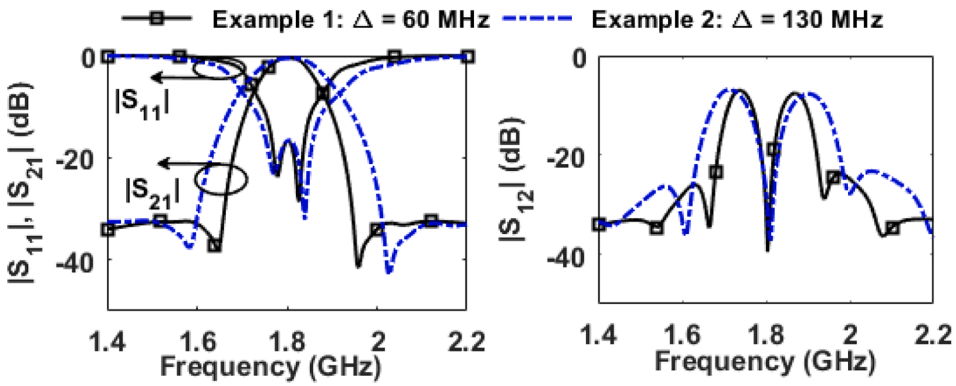

Fig. 5. Numerical simulation results of quasi-elliptic NBPF with different equiripple bandwidth (Δ) at static state. Coupling matrix values are obtained by optimization and are given as: $M_{s1} = 1.3440$, $M_{12} = 1.3055$, $M_{23} = 1.4971$, $M_{3L} = 1.3301$, $M_{1L} = -0.1120$. Progressive phase shift: $\Delta\varphi = 75^{\circ}$.

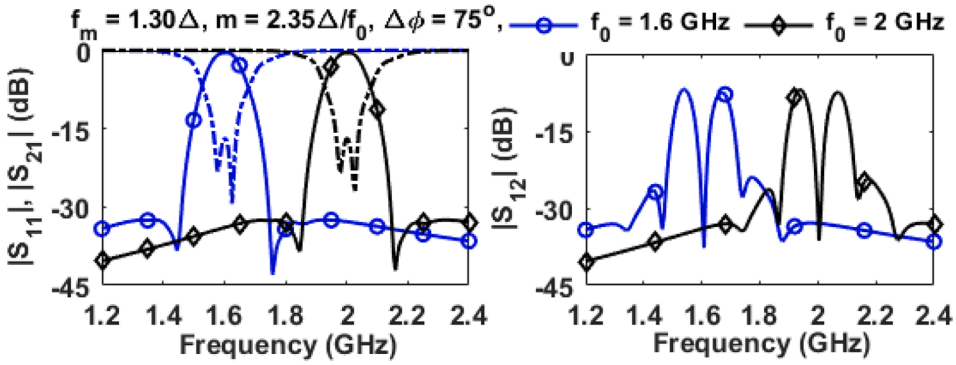

Fig. 6. Numerical simulation results of quasi-elliptic NBPF with reconfigurable passband response. Coupling matrix values are obtained by optimization and are given as: $M_{s1} = 1.3440$, $M_{12} = 1.3055$, $M_{23} = 1.4971$, $M_{3L} = 1.3301$, $M_{1L} = -0.1120$. Progressive phase shift: $\Delta\varphi = 75^{\circ}$.

$S_{12}|$) is > 40 dB and input/output return loss is > 16 dB at center frequency. As indicated by equation (6), m is proportional to Δ, therefore, when Δ is chosen as 60 MHz and 100 MHz at $f_0 = 1.8$ GHz, desired values of m are 0.078 and 0.13, respectively.

Fig. 6 illustrates the numerically calculated frequency response of the fully reconfigurable quasi-elliptic NBPF. The passband tunability of quasi-elliptic NBPF is achieved by adjusting the resonant frequency of time-modulated resonators. In these simulations, the modulation parameters are chosen using (6). Results show that the passband center frequency is tuned from 1.60 GHz to 2 GHz while maintaining input/output RL > 16 dB, forward transmission IL < 0.5 dB and backward IX > 40 dB at each tuning state.

2.2. Design guide of proposed quasi-elliptic NBPF

Based on the filter specifications (such as center frequency, bandwidth, in-band return loss characteristics and location of transmission zeros at static state), numerical simulations have been carried out using analytical spectral S-parameters equations shown in (2)-(5). The modulation parameters have chosen using (6). The sequential design steps of the proposed quasi-elliptic NBPF are summarized as follows:

(a) Define filter specification such as center frequency (f_0), bandwidth (Δ) at static state (without modulation), in-band return loss (RL) characteristics, and location of TZs.
(b) Construct coupling matrix values ($\mathbf{M}_{s1} = M_{s1}U$, $\mathbf{M}_{12} = M_{12}U$, $\mathbf{M}_{23} = M_{12}U$, $\mathbf{M}_{3L} = M_{3L}U$, and $\mathbf{M}_{1L} = M_{1L}U$) according to desired RL and TZ locations [18]. U represents a unitary matrix.
(c) Calculate modulation parameters (f_m, m, Δφ) using (6).
(d) Using modulation parameters, calculate λ_i using (2) for all frequencies.
(e) Calculate and plot frequency responses of the proposed NBPF using (3)-(5) to achieve desired non-reciprocity response in the passband.
(f) Once the desired non-reciprocal response is achieved, calculate admittance/impedance inverter values using coupling matrix (M_{s1}, M_{12}, M_{23}, M_{3L}, and M_{1L}) and slope parameters of time-modulated resonators. The time-modulated resonators can be implemented either using lumped elements (such as inductors and varactor diodes) or microstrip lines (such as transmission lines and varactor diodes). The calculation of admittance inverters will follow same as the conventional filter design approach [20].
(g) Construct overall circuit of the NBPF by implementing admittance/impedance inverters with appropriate physical structure. Finally optimize physical dimensions using 3-D electromagnetic simulator.

3. Experimental results

For experimental proof-of-concept, a prototype of a microstrip line quasi-elliptic NBPF is designed and manufactured on Taconic substrate with dielectric constant of 2.2 and thickness of 0.787 mm. NBPF was designed to have Δ = 68 MHz at $f_0 = 1.80$ GHz. Fig. 7 shows microstrip line implementation of the proposed quasi-elliptic NBPF. Firstly, according to filter specifications (such as center frequency, bandwidth, return loss characteristics, transmission zeros locations), a reciprocal filter is designed using coupling shown in Fig. 1(a). Once coupling matrix values are determined, the admittance inverter values are obtained using impedance scaling, bandpass transforming to center frequency and fractional bandwidth, and slope parameter of resonator. After obtaining all the parameters of equivalent circuit shown in Fig. 7(a), the

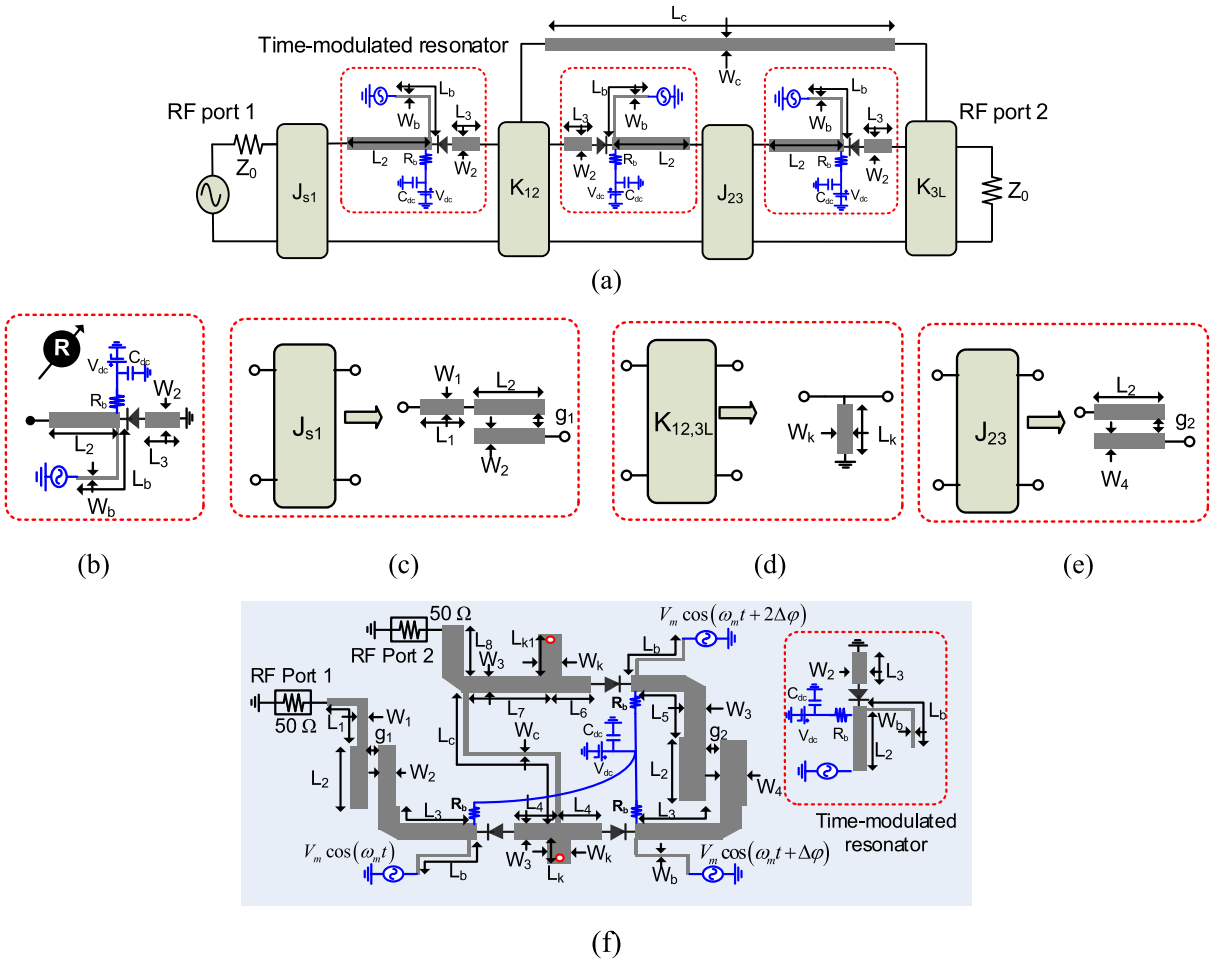

Fig. 7. (a) Circuit equivalent of proposed quasi-elliptic NBPF, (b) time-modulated resonator, (b) ~ (e) inverters implementation using transmission lines, and (f) overall microstrip line implementation of proposed quasi-elliptic NBPF. Physical dimensions: $W_1 = 0.9$, $L_1 = 12.1$, $W_2 = 1.1$, $L_2 = 10.76$, $g_1 = 0.14$, $W_3 = 1.36$, $L_3 = 16$, $L_4 = 5.72$, $W_k = 1.4$, $L_k = 1.3$, $L_{k1} = 7$, $W_4 = 1.71$, $g_2 = 0.7$, $L_5 = 16$, $L_6 = 1.4$, $L_7 = 10$, $L_8 = 9$, $W_c = 0.5$, $L_c = 34.9$, $W_b = 0.6$, $L_b = 23$, $C_{dc} = 100$ pF and $R_b = 10$ kΩ. Unit: millimeter (mm). Varactor SMV: 1233-079LF from Skyworks Inc.

time-modulated resonators and static inverters are implemented with transmission lines (TLs) and varactor as shown in Fig. 7(b) ~ (d). In this work, the time modulated resonators are realized with quarter-wavelength TL terminated with varactor diode SMV 1233-079LF from Skyworks Inc [21], as shown in Fig. 7(b). The required resonant frequency of time-modulated resonators can be obtained by changing lengths L_2, L_3, and width W_2. The progressive phase shift modulation signal is applied to varactor diode through TL elements W_b and L_b. The admittance inverter (J_{s1}) between input port 1 and resonator 1 is implemented through TL elements W_1, L_1 and coupled line elements W_2, L_2, g_1 as shown in Figure (c). Similarly, impedance inverters (K_{12} and K_{3L}) between resonators 1 and 2, and between resonator 3 and output port 2 are implemented through short-circuit shunt stub with physical parameters W_k and L_k as shown in Fig. 7(c) whereas admittance inverter (J_{23}) between resonators 2 and 3 is realized through coupled line elements W_4, L_2 and g_2 as shown in Fig. 7(d). The cross-coupling (M_{1L}) between resonator 1 and output port 2 is obtained through TL of physical parameter W_c and L_c. The layout of overall microstrip line implementation of the proposed quasi-elliptic NBPF is shown in Fig. 7(f) with physical dimensions. The co-simulation is conducted using ANSYS HFSS and PathWave ADS to optimize physical parameters. The modulation parameters of the proposed quasi-elliptic NBPF are estimated using (6) as follows: $f_m = 85$ MHz, $m = 0.1109$ and $\Delta\varphi = 75°$.

Fig. 8 shows the simulation and measurement results, demonstrating a good agreement between simulated and measured responses. The center frequency of quasi-elliptic NBPF is tuned from 1.65 GHz to 1.95 GHz achieving tuning ratio of 1.182:1, by varying dc-bias voltage from 0 to 6.5 V. While a finite number of frequency responses are shown in Fig. 8, it should be noted that the passband frequency can be continuously adjusted. The minimum in-band IL in forward transmission varies between 3.42 and 4.8 dB and IX in reverse direction ranges from 27 dB to 34.5 dB, while maintaining in-band return loss > greater than 12 dB throughout entire tuning range. Throughout all tuning states, the proposed tunable NBPF generates two TZs, resulting in quasi-elliptic response. The forward transmission IL is mainly due to parasitic resistance of varactor diode. The varactor diode parasitic resistance increases as the DC-bias voltage of varactor diode is tuned toward to lower value (such as 0 V). The passband frequency of the proposed quasi-elliptic NBPF is tuned by changing the varactor diode bias voltage. As shown in Fig. 8, the passband frequency is tuned toward lower frequency by changing dc-bias voltage of varactor of varactor diode toward lower value. Therefore, the forward transmission IL increases when the passband frequency is tuned toward a lower frequency because of higher parasitic resistance at lower DC-bias voltage.

Fig. 9 shows the measured response of quasi-elliptic NBPF under with and without modulation condition. When modulation is turned off, the filter provides reciprocal filter response ($|S_{21}| = |S_{12}|$) with forward IL of 2.73 dB and input and output ports matching are greater than 25 dB at center frequency of 1.80 GHz. When modulation is turned, the proposed filter provides non-reciprocal response ($|S_{21}| \neq |S_{12}|$) where

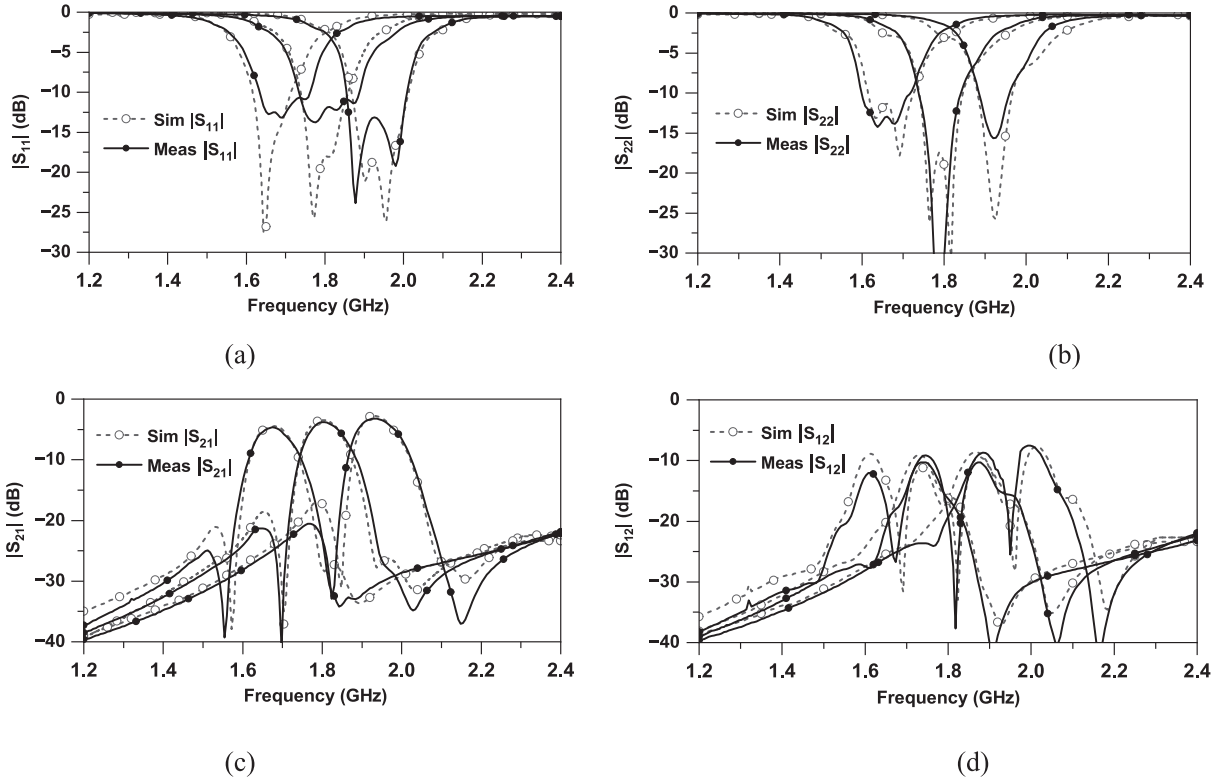

Fig. 8. Simulation and measurement results of fabricated quasi-elliptic NBPF: (a) input return loss ($|S_{11}|$), (b) output return loss ($|S_{22}|$), (c) forward transmission ($|S_{21}|$), and (d) reverse transmission ($|S_{12}|$).

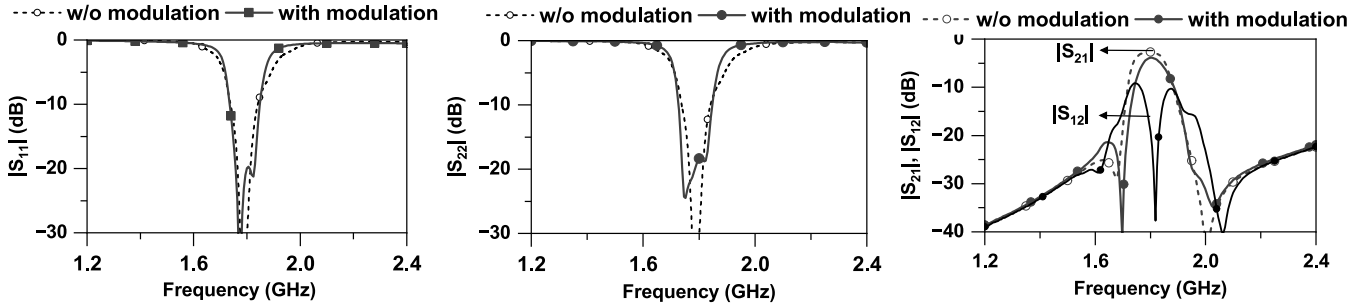

Fig. 9. Measurement results of quasi-elliptic NBPF with and without modulation.

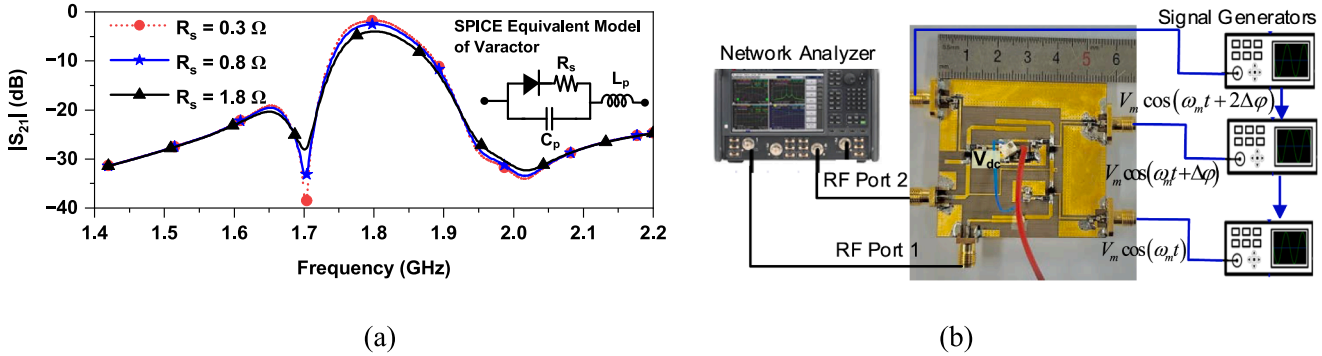

Fig. 10. (a) Simulation results of quasi-elliptic NBPF with different values of parasitic resistance R_s in SPICE model of varactor SMV 1233-079LF and (b) photograph of fabricated quasi-elliptic NBPF with measurement setup. Other parasitic parameters of varactor diode: $C_p = 0.5$ pF and $L_p = 0.7$ nH [21].

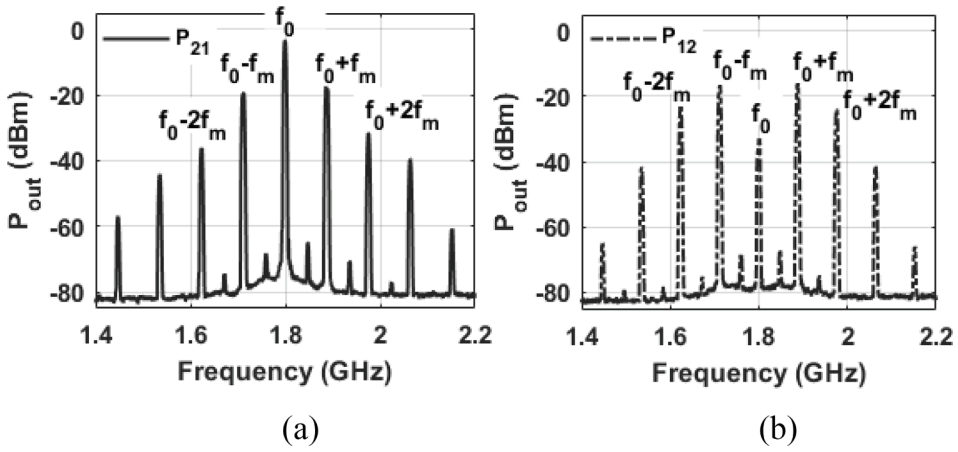

Fig. 11. Measured output harmonic spectrum of quasi-elliptic NBPF when one-tone signal at $f_{RF} = 1.80$ GHz and $P_{in} = 0$ dBm is applied to input port: (a) forward direction P_{21} (b) reverse direction P_{12}.

Table 1
Performance comparison with state-of-the-art.

	FTR (GHz)	RL (dB)	IL (dB)	BW_{3dB} (MHz)	IX @f_0 (dB)	Technology	TVR	A	QE
[6]	0.19	15	1.50	30	20.2	Lumped	3	Y[a]	N
[7]	0.136 ~ 0.163	>14	3.7 ~ 4.1	27.5	21 ~ 26	Lumped	3	N	N
[8]	0.150	>17	1.8	140	18	Lumped	3	Y[a]	N
[9]	0.15	>14	3.20	20	28.6	Lumped	3	N	N
[10]	0.57 ~ 0.724	>15	4.8 ~ 6.8	37.5 ~ 73.9	21 ~ 35	Lumped	4	Y	Y
[13]	0.88 ~ 1.03	>10.9	3.9 ~ 4.6	NA	20	Microstrip	3	N	N
[15]	1.64 ~ 1.97	>11	3.94 ~ 4.92	87 ~ 97	20	Microstrip	3	N	N
[16]	1.46	>15.2	3.10	160	20.2	Microstrip	2	N	N
[17]	0.27 ~ 0.31	>10	1.7 ~ 4.3	41.5	15.4 ~ 30.9	Lumped	4	N	Y
[18]	1.08	>12	3.6	130	36.2	Microstrip	4	N	Y
[19]	0.725	>15	3.2	90	6.8 ~ 62.1	Microstrip	4	N	Y[b]
This work	**1.65 ~ 1.95**	**> 12**	**3.20 ~ 4.82**	**102 ~ 115**	**22.1 ~ 34.5**	**Microstrip**	**3**	**Y**	**Y (Two TZs)**

A = Nonreciprocal frequency response analysis using analytical design equations.
BW_{3dB} = 3-dB bandwidth of forward transmission ($|S_{21}|$).
QE: Quasi-elliptic response.
[a] Spectral *S*-parameters without cross-coupling.
[b] Balanced quasi-elliptic NBPF.

forward transmission IL is 3.98 dB and reverse IX is 34 dB and input/output return losses are higher than 17 dB at center frequency of 1.80 GHz.

To investigate the cause of the forward transmission IL, we performed simulation of quasi-elliptic NBPF using SPICE model of varactor diode SMV 1233-079LF [21] and results are shown in Fig. 10(a). The forward transmission IL is mainly due to a fraction of inter-harmonic spectral power conversion to IM products and parasitic resistance (R_s) of varactor diode. A fraction of inter-harmonic spectral power conversion to IM products generates IL of 0.7 dB and the rest of IL is due to parasitic resistance R_s of the varactor diode. As the value of R_s increases, the forward transmission IL also increases. The IL can be improved if varactor diode with low parasitic resistance (high *Q*-factor varactor diode) is used.

Fig. 11 shows the measured output harmonic spectrum of the proposed quasi-elliptic NBPF. Due to the nonlinear behavior of the modulated varactors, output harmonic spectrum can be observed. When one tone RF power of $f_0 = 1.80$ GHz and $P_{in} = 0$ dBm is applied to RF port 1, the output power of −3.64 dBm at f_0, and 18.8 dBm/17.8 dBm at f_0-f_m/$f_0 + f_m$ are observed at RF port 2. Similarly, when RF power $P_{in} = 0$ dBm is applied to RF port 2 in reverse direction, the output power of −34.4 dBm at f_0 and 15.5 dBm/16.2 dBm at f_0-f_m/$f_0 + f_m$ are obtained at RF port 1, providing reverse isolation of 34.5 dB.

The performance of the proposed NBPF is compared with the state-of-art as shown in Table 1. The work [10,17] demonstrated lumped element NBPF with quasi-elliptic response in forward direction transmission. However, works [10,17] require at least four time-modulated resonators and four separate low pass filters to separate RF signal and modulation signal, resulting in complexity of modulation circuit. In contrast, the proposed work demonstrated microstrip line NBPF with quasi-elliptic response in the forward direction transmission using only three-time modulated resonators. In addition, by directly applying the modulation signal to varactor diode through the TL, the proposed NBPF simplifies the modulation circuit by eliminating the need to separate low pass filter. The proposed work also offers analytical design equations incorporating cross-coupling that allow to gain analytical insight into the distribution of RF signal among IM products generated in time-modulated resonators. In addition, analytical design equations proposed in this work provides easy extraction of modulation parameters that can be directly used in design and experimental validation of tunable quasi-elliptic NBPF with enhanced frequency selective characteristics.

4. Conclusion

This paper presented the design and implementation of a tunable NBPF with a quasi-elliptic transfer response. An empirical relationship between modulation parameters and filter specifications was established to achieve quasi-elliptic bandpass response in forward direction and a highly attenuated response in reverse direction. For experimental validation, a prototype of microstrip line quasi-elliptic NBPF was designed, manufactured, and measured. The fabricated prototype exhibited

passband center frequency tuning range of 1.182:1, with minimum in-band insertion loss < 4.8 dB and two TZs in forward transmission, isolation level up to 34.5 dB in reverse direction and RL > 12 dB in all tuning state. The proposed quasi-elliptic NBPF can be applied in various applications of wireless communication systems. Since the proposed quasi-elliptic NBPF combines functionalities of quasi-elliptic tunable filter and isolator within single circuit, miniaturized wireless transceiver systems can be designed using the proposed NBPF that allows reduction of components both transmitter and receiver by performing filtering and isolation operations.

CRediT authorship contribution statement

Girdhari Chaudhary: Writing – review & editing, Writing – original draft, Validation, Methodology, Investigation, Data curation, Conceptualization. **Yongchae Jeong:** Supervision, Project administration, Methodology, Funding acquisition.

Declaration of competing interest

The authors declare that they have no known competing financial interests or personal relationships that could have appeared to influence the work reported in this paper.

Data availability

Data will be made available on request.

Acknowledgment

This research was supported by National Research Foundation of Korea (NRF) grant funded by Korea Government (MSIT: Ministry of Science and ICT) (No RS-2023-00209081) and in part by Basic Science Research Program through the NRF grant funded by Ministry of Education (2019R1A6A1A09031717).

References

[1] Hong S, Brand J, Choi J, Jain M, Mehlman J, Katti S, Levis P. Application of self-interference cancellation in 5G and beyond. IEEE Communication Magazine 2021; 14:114–21.
[2] Zhou J, Reiskarimian N, Diakonikolas J, Dinc T, Chen T, Zussman G, et al. Integrated full duplex radios. IEEE Communication Magazine 2017;55(4):142–51.
[3] Fay CE, Comstock RL. Operation of the ferrite junction circulator. IEEE Transactions on Microwave Theory Techn 1965;13(1):15–27.
[4] Seewald CK, Bray JR. Ferrite-filled anti-symmetrically biased rectangular waveguide isolator using magnetostatic surface wave modes. IEEE Transactions on Microwave Theory Techn 2010;58(6):1493–501.
[5] Estep NA, Sounas DL, Alu A. Magnetless microwave circulators based on spatiotemporally modulated rings of coupled resonators. IEEE Transactions on Microwave Theory Techn 2016;64(2):502–18.
[6] Wu X, Liu X, Hickle MD, Peroulis D, Gomez-Dıaz JS, Alvarez Melcon A. Isolating bandpass filters using time-modulated resonators. IEEE Transactions on Microwave Theory Techn 2019;67(6):2331–45.
[7] Simpson D, Psychogiou D. Magnet-less non-reciprocal bandpass filters with tunable center frequency. Proc European Microwave Conference 2019:460–3.
[8] Dutta P, Kumar GA, Ram G. Numerical design of non-reciprocal bandpass filters with the aid of 3D coupling matrix for 5G bands. IEEE Trans. Circuits and Systems-II, Express Briefs 2022;69(7):3334–8.
[9] Dutta P, Kumar GA, Ram G. Numerical insight into the origin of nonreciprocity and performance enhancement in nonreciprocal bandpass filters using evolutionary algorithm. IEEE Trans Computer-Aided Design of Integrated Circuits and Systems 2023;42(7):2428–32.
[10] Zhang Z, Psychogiou D. Incorporating directionality in transversal resonator based bandpass filters with tunable transfer function characteristics. IEEE Trans Circuits and Systems-I Regular Papers 2023;70(12):5194–207.
[11] Wu X, Nafe M, Alvarez Melcon A, Gomez-Dıaz JS, and Liu X, A non-reciprocal microstrip bandpass filter based on spatio-temporal modulation. in 2019 IEEE MTT-S International Microwave Symposium. Dig., (IMS), 2019; 9–12.
[12] Shiarzi M, Chatzichristodoulou D, Quddious A, Shoaib N, Psychogiou D, Nikolaou S, et al. Non-reciprocal bandpass filter with tunable center frequency and constant fractional bandwidth. IEEE MTT-S International Microwave Filter Workshop 2021:252–4.
[13] Wu X, Nafe M, Alvarez Melcon A, Gomez-Diaz JS, Liu X. Frequency tunable non-reciprocal bandpass filter using time-modulated microstrip $\lambda_g/2$ resonators. IEEE Trans. Circuits and Systems-II: Express Briefs 2021;68(2):667–71.
[14] Alvarez Melcon A, Wu X, Zang J, Liu X, Gomez-Dıaz JS. Coupling matrix representation of nonreciprocal filters based on time modulated resonators. IEEE Transactions on Microwave Theory Techn 2019;67(12):4751–63.
[15] Chaudhary G, Jeong Y. Frequency tunable impedance matching nonreciprocal bandpass filter using time-modulated quarter-wave resonators. IEEE Trans Industrial Electronics 2022;69(8):8356–65.
[16] Chaudhary G, Jeong Y. Nonreciprocal bandpass filter using mixed static and time-modulated resonators. IEEE Microwave Wireless Components Letters 2022;32(4): 297–300.
[17] Simpson D, Psychogiou D. Fully-reconfigurable non-reciprocal bandpass filters. IEEE International Microwave Symposium Dig 2020.
[18] Chatzichristodoulou D, Arain S, Pavlou C, Vassiliou L, Psychogiou D, Nikolaou S, et al. Spatiotemporal modulated three-pole nonreciprocal quasi-elliptic bandpass filter. Proc European Microwave Conference 2022:289–92.
[19] Simpson D, Vryonides P, Nikolaou S, Psychogiou D. Non-reciprocal balanced bandpass filters with quasi-elliptic response. IEEE Trans. Circuits and Systems-II: Express Briefs 2022;69(12):5159–62.
[20] Cameron RJ, Mansour R, and Kudsia CM, *Microwave Filters for Communication Systems: Fundamentals, Design and Applications*, Hoboken, NJ, USA: Wiley, 2007.
[21] SMV123x series: *Hyper-abrupt junction tuning varactors*, Skyworks Solutions, Inc., Nov. 2018.